Estimation and Control of a Quadrotor Attitude

Bernardo Sousa Machado Henriques
Mechanical Engineering Department, Instituto Superior Técnico, Lisboa, Portugal
E-mail: henriquesbernardo@gmail.com

***Abstract*—The aim of the present work is to estimate and control the attitude of a quadrotor aircraft prototype using solely inexpensive sensors: 3-axes accelerometer, 3-axes gyroscope, 2-axes compass and a range finder. We first introduce the concept of the quadrotor. The characteristics of the prototype are estimated and the dynamics and kinematics models of the quadrotor concept are developed. To complete the model, the actuators and the sensors are modeled too. This led to the implementation of the model in *Simulink*. After linearizing the model around the operating point, a linear state space system was obtained and used to obtain a 12 states LQR controller using ideal sensors. Closing the loop with that controller generated attitude data which was used to tune the different estimators considered. The Complementary Filter and the different Kalman filters as the linear and expended Kalman filters are tested and compared. An 8 states LQR controller using ideal sensors is then tuned to control the attitude and height of the quadrotor in in discrete states. The LQR is also tested with feedback from the chosen estimator, the EKF. Then, the estimator proves to be well tuned after being implemented on the prototype and tested in open loop considering the operating conditions: all motors turned on. Finally the results suggest that the discrete LQR controller along with the EKF are a good strategy for estimating and controlling the attitude of a quadrotor.**

***Index Terms*—Quadrotor, VTOL, Extended Kalman filter, Complementary filter.**

I. Introduction

The quadrotor is a rotoracraft vehicle capable of vertical landing and take-off (VTOL). The concept of quadrotors has been mostly developed by the military in the past century, motivated by the search for alternatives to traditional helicopters. However, in recent years, the advance of miniaturization and maturing of technologies bolstered the interest in unmanned quadrotors in the academic milieu, where these vehicles appear as challenging platforms to develop new solutions for control, estimation, communication problems, 3D orientation and navigation algorithms.

Mini UAV, with limited payload require small sensors, usually inexpensive. The objective is to control and estimate the attitude of a quadrotor vehicle using solely inexpensive sensors to have a functional platform able of hover flight. The available sensors are: three axes *ADXL330* accelerometer, two axes *LPR530AL* and one axis *LY530ALH* gyroscopes, both from the 6DOF IMU from *Sparkfun*, two axes *Honeywell HMC6352* compass and a *Sharp DP2D12* range finder.

To obtain an adequate controller and estimator, the model of the quadrotor is derived comprising the model of the sensors and the model of the actuators. These two models use experimental results to determine the necessary parameters. This provides more realism to the simulations. The obtained model is linearized and through simulations a 12 states LQR controller is used to generate data concerning the attitude, which is then used to tune and compare estimation approaches. An 8 states LQR controller is then obtained for stabilization purposes only and it is used with estimation feedback in simulations. Finally the chosen estimator is then implemented on the prototype. This will allow us to draw some conclusions about the available sensors and the stabilization techniques.

II. Model of the Quadrotor

A. Definitions

To describe the movement of the quadrotor and its attitude a reference frame, called NED frame, centered on O, is set on the ground and points towards North, East and Down; it is considered to be inertial. A second frame is fixed on the quadrotor and centered on Oc, the center of mass of the quadrotor, thus called Body-fixed frame, shown in Figure 1. Vectors expressed in the inertial frame are marked with the superscript ^{I} and vectors expressed in the body fixed frame have the superscript ^{B}.

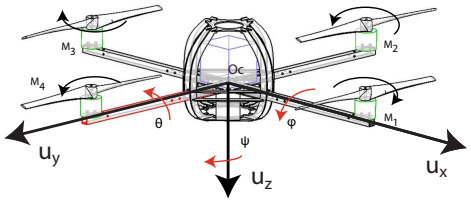

Fig. 1. Body-Fixed Frames.

The position of the quadrotor, denoted $\mathbf{P}^B = [X, Y, Z]^T$, corresponds to the displacement from O to Oc. The velocity of the quadrotor is expressed in the body-fixed frame as: $\mathbf{V}^B = [U, V, W]^T$. The rotation of the body-fixed frame relatively to the inertial frame defines the attitude of the craft. In aeronautic literature Euler angles are normally used: ϕ, θ and ψ. The attitude is described by: $\mathbf{\Psi} = [\phi, \theta, \psi]^T$. The angular velocities in the body-fixed frame are written: $\mathbf{\Omega}^B = [P, Q, R]^T$ with P, Q, R corresponding respectively to roll, pitch, yaw motions.

Quadrotors have four identical rotors and the propellers have a fixed angle of attack. As shown on Figure 1 the blades are paired and each pair rotates in a different direction. Motors *M1* and *M3* have a clockwise rotation when looked from above whilst motors *M2* and *M4* have a counter-clockwise rotation. To obtain the maneuvers depicted in Figure 1 the speed of each motor is adjusted. The angular speeds of the motors are written $\omega = [\omega_1, \omega_2, \omega_3, \omega_4]^T$. Figure 2 presents these adjustments and their respective effect.

The rolling motion corresponds to a rotation of the quadrotor about the u_x axis; it is obtained when ω_2 and ω_4 are changed. For a positive rolling, ω_4 is decreased while ω_2 is increased. The contrary will produce a negative rolling action; both are depicted in cases *(a)* and *(b)*. The pitch motion, around u_y axis, is obtained as the rolling motion. For a positive pitch, ω_3 is decreased while ω_1 is increased. The contrary will produce a negative pitch action; both are depicted in cases *(c)* and *(d)*.

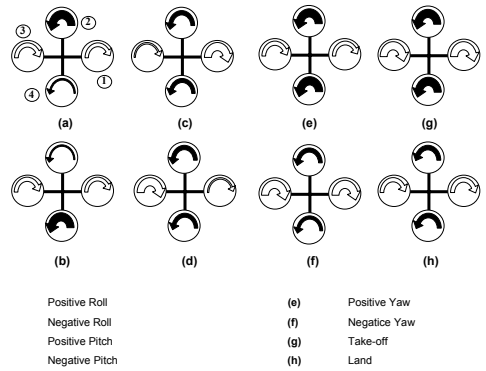

Fig. 2. Quadrotor Rotation System (from [1]).

The yaw motion corresponds to a rotation of the quadrotor about the u_z axis; it is produced by the difference in the torque developed by each pair of propellers. Since the propellers are paired, two create a clockwise torque and two a counter clockwise one; by varying the angular speed of one pair over the other, the net torque applied to the aircraft changes which results in the yaw motion as shown in cases *(e)* and *(f)*.

To perform a vertical takeoff and landing, quadrotors must be able to move vertically. As shown in cases *(g)* and *(h)*, this movement is obtained by equally augmenting or diminishing the angular speed of all motors. Positive pitch or roll angles produce respectively negative and positive translational motion along u_x and u_y.

B. Dynamics and Kinematics of a Quadrotor

The dynamics and kinematics of the quadrotor can be summarized in equation (1)-(4) in accordance to [2]:

$$\dot{\mathbf{P}}^I = \mathbf{S}^{\mathbf{T}}\mathbf{V}^B \tag{1}$$

$$\mathbf{I}\dot{\mathbf{\Omega}}^B = -\mathbf{\Omega}^B \times \mathbf{I}\mathbf{\Omega}^B + \mathbf{M}^B \tag{2}$$

$$\dot{\mathbf{V}}^B = \frac{1}{m}\mathbf{F}^B + \mathbf{S}^{\mathbf{T}}\mathbf{g}^I - \mathbf{\Omega}^B \times \mathbf{V}^B \tag{3}$$

$$\dot{\mathbf{\Psi}}^B = \mathbf{T}\mathbf{\Omega}^B \tag{4}$$

Equation (1) defines the linear movement of the quadrotor as the derivative of the position. The matrix $\mathbf{S}$ is the rotation matrix which expresses a vector from the inertial frame to the body-fixed frame. Equation (2) contains the input moments, $\mathbf{M}^B$, developed by the four propellers. The inertia matrix $\mathbf{I}$ is diagonal due to the symmetry of the quadrotor. Equation (3) is derived from the second law of Newton, where $\mathbf{F}^B$ are the forces of thrust developed by the propellers, $\mathbf{g}^I = g_0[0,0,1]^T$ is the gravity vector with $g_0 = 9.81m/s^2$. Equation (5) shows how the moments and forces are calculated considering K_T and K two constants characteristic of the propellers and d_{cg} the position of the propeller relative to the center of mass.

$$\begin{aligned} F_i &= K_T\omega_i^2 \\ M_x &= (F_2 - F_4)d_{cm} \\ M_y &= (F_1 - F_3)d_{cm} \\ M_z &= (F_1 + F_3 - F_2 - F_4)K \end{aligned} \tag{5}$$

Equation (4) presents the kinematics of the attitude. The matrix $\mathbf{T}$ is written in equation (6):

$$\mathbf{T} = \begin{bmatrix} 1 & \tan\theta\sin\phi & \tan\theta\cos\phi \\ 0 & \cos\phi & -\sin\phi \\ 0 & \sin\phi/\cos\theta & \cos\phi/\cos\theta \end{bmatrix} \tag{6}$$

C. Model of the Sensors

To complete the model of the quadrotor prototype, the gyroscopes, accelerometers, compass and range finder shall be modeled too. Real data measurements are used to estimate the characteristics of the noise corrupting the sensor measurements.

1) Gyroscopes: The *LPR530AL* sensor is used to measure angular velocities corresponding to pitch and roll rates, P and Q, and the *LY530ALH* sensor is used for yaw motion, R. Both sensors are from *STMicroelectronics* and present the same dynamics and governing equations; as suggested by [2] and [3], the gyroscope is mostly affected in two ways: a stochastic Gaussian noise component, $\mu_{\mathbf{g}}$, and a slowly time-varying non-stochastic bias, $\mathbf{b}(\mathbf{t})_{\mathbf{g}}$, corrupt the readings. Therefore the gyroscopes measurement can be written:

$$\overline{\mathbf{\Omega}}^B = \mathbf{\Omega}^B + \mu_{\mathbf{g}} + \mathbf{b}_{\mathbf{g}}. \tag{7}$$

In flight conditions, the four motors are turned on, which causes undesired noise to corrupt the measurements. Practical measurements, showed that noise affecting the gyroscopes has spectral power: $\mu_{\mathbf{g}} = [0.245, 0.301, 0.196]^T(^\circ/s)^2/Hz$.

2) Accelerometer: The accelerometer is used to measure the direction of the gravity vector, $\mathbf{g}^I$, in order to define the pitch and roll angles; let $\overline{\mathbf{a}}^B$ denote the accelerometer measurement vector. It is suggested that $\overline{\mathbf{a}}^B = \mathbf{S}\mathbf{g}^I - \mathbf{a}^B$. The accelerometer is not only sensitive to the gravity but also to accelerations due to its movement, written $\mathbf{a}^B$. This model comes from the fact that in a horizontal position standing still, the accelerometer shows that $\overline{a_z} = g_0$ and in a free fall situation, when the acceleration due to the movement is $\mathbf{a_z} = \mathbf{g}^I$, the accelerometer is intended to output $\overline{a_z} = 0$. When considering the hover flight, according to [2], for the chosen frame system and including a Gaussian noise perturbation, one can approximate the model to equation (8), where a centripetal and tangential accelerations appear due to the sensor being located at $\mathbf{r} = [0, 0, -5.2cm]^T$ from the center of mass of the prototype.

$$\overline{\mathbf{a}}^B = \mathbf{S}\mathbf{g}^I + \dot{\mathbf{\Omega}} \times \mathbf{r} + \mathbf{\Omega} \times (\mathbf{\Omega} \times \mathbf{r}) + \mu_{\mathbf{a}} \tag{8}$$

To identify how the vibrations of the motors corrupt the accelerometer measurements, sensor measurements are taken with the motors on and with the motors off. The results proved that there is no bias affecting the measurements and the noise spectral power is: $[0.0932, 0.0885, 0.0302]^T(m/s^2)^2/Hz$. The model is an approximation valid only for near hover situations, where the acceleration of the quadrotor due to its movement is not significant.

3) Compass: The *Honeywell HMC6352* compass is a sensor designed to detect the magnetic North direction, written $\mathbf{N}^I = [1, 0, 0]^T$. Let $\overline{\mathbf{N}}^B$ denote the sensor measurement. According to [4] the model of the sensor can be approximated to (9):

$$\overline{\mathbf{N}}^B = \mathbf{S}\mathbf{N}^I = \begin{bmatrix} \cos\theta\cos\psi \\ \cos\psi\sin\phi\sin\theta - \cos\phi\sin\psi \\ \cos\psi\cos\phi\sin\theta + \sin\phi\sin\psi \end{bmatrix} \tag{9}$$

However because the sensor has only two sensing axes, it is approximated to equation (10). The compass measurements are affected by soft iron and hard iron distortions: according to [5], hard iron distortions are caused by the presence of permanent magnets and magnetized iron or steel, they produce a constant additive error regardless of the orientation. Soft iron distortions are similar to hard iron distortions but the error varies with the orientation. As a consequence, the hard iron distortions are included in a constant bias term, $\mathbf{b_m}$, but the soft iron effect cannot be easily accounted for and is neglected. In addition, the model is affected by a Gaussian measurement noise, $\mu_\mathbf{m}$.

$$\overline{\mathbf{N}}^{\mathbf{B}} = \begin{bmatrix} \cos\psi \\ -\sin\psi \\ 0 \end{bmatrix} + \mu_\mathbf{m} + \mathbf{b_m} \tag{10}$$

The approximation is only valid near hover situations where the tilt and roll angles are not significant. to verify whether the motors increase the measurement noise of the compass, they were turned on one by one and the compass measurements were obtained. The test shows that the motors have little influence on the compass. The spectral power of the noise measurement was measured to be $0.125deg^2/Hz$.

4) Range Finder: The purpose of the range finder is to provide the quadrotor with a measurement of the height, Z. The measurement is written $\overline{z}^B$ in meters and corresponds to a distance between the center of mass of the quadrotor and the floor along u_z. This approximation is valid only in a hover situation where tilt and roll are small. The sensor has a nonlinear behavior: the output voltage of the sensor is a function of the inverse of the measured distance; as a consequence, the sensor presents more accurate readings for smaller distances. In addition, a Gaussian noise term, μ_z, corrupts the readings. Since the sensor is not located on the center of mass of the quadrotor, there is an offset in the measurement, or a constant bias b_z. Equation (11) corresponds to the model of the sensor:

$$\overline{z}^B = Z + \mu_z + b_z \tag{11}$$

The prototype was set at different distances from the floor as presented in Figure 3 to identify the behavior of the sensor. The Figure presents also the identified curve: $\overline{z}^B = 14882/(Sensor_{output} + 91.8) - 0.8$ in cm. Experimentally it

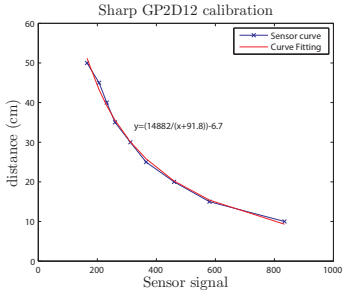

Fig. 3. Identification of the Range Finder.

is noticed that the sensor is not affected by any bias. The noise affecting the sensor is estimated for low heights and is neglectable.

D. Model of the Actuators

The actuators are the components responsible for applying forces on the system to bring it to a desired state. In this case the actuators are the motors and propellers. In Figure 4 the actuator set is schematized. A micro controller is connected to the speed controller, which receives the PWM signal and controls the motor making the propeller spin, which generates the forces and moments of equation (5).

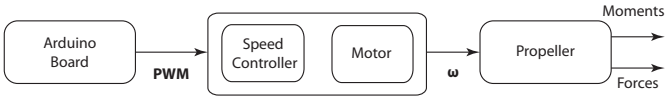

Fig. 4. Configuration of the Actuators.

The two coefficients, K and K_T are dependent on the propeller properties: $K_T = 1.46 \times 10^{-5} kg.m.rad^{-2}$ and $K = K_M = 0.026m$. The PWM signal, a square digital signal, is a common method to provide an analog signal with digital means [1]; the processor uses a normalized $50Hz$ square wave to code the signal as a pulse width varying from 1 ms to 2 ms. Speed controllers are used to turn the PWM signal into a triphasic signal fed to the brushless DC motors.

The motor i receives the triphasic signal corresponding to an order of angular velocity ω_i. The model of the motor, which receives a PWM reference and develops an angular velocity, is approximated to a first order system:

$$\frac{\omega_i}{PWM_i} = \frac{k_i}{\tau s + 1} \tag{12}$$

where: τ is the time constant of the system. k_i is the dc gain.

The four motors are expected to present different characteristics partly because the speed controllers used are not identical. The actuators hold nonlinear behaviors as the dead zone and a quantizer. To define the dead zone, PWM_i^d,the PWM signal is increased until the motor starts to spin. Table I presents the results. The quantizer is originated by the function used to set the PWM signal which only accepts integer values in units of μs.

TABLE I
DEAD ZONE OF THE MOTORS

Motor	PWM_i^d in μs
M_1	1179
M_2	1184
M_3	1190
M_4	1260

To define the static gain of equation (12), a tachometer is used to measure the stationary response of the motor to different PWM values. Figure 5 presents the estimation results. The curves are then identified as a second order polynomial. Because the hover condition corresponds to all propellers generating enough thrust to lift the quadrotor, the operating point can be obtained in terms of ω: $\omega_i^{0^2} = \frac{mg_0}{4K_T}$; where $m = 0.987kg$ is the mass of the prototype. Using that information, the operating point in terms of PWM is obtained. The

[1]A brief introduction to the PWM signal is presented in the documents supporting the Arduino project: http://www.arduino.cc/en/Tutorial/PWM

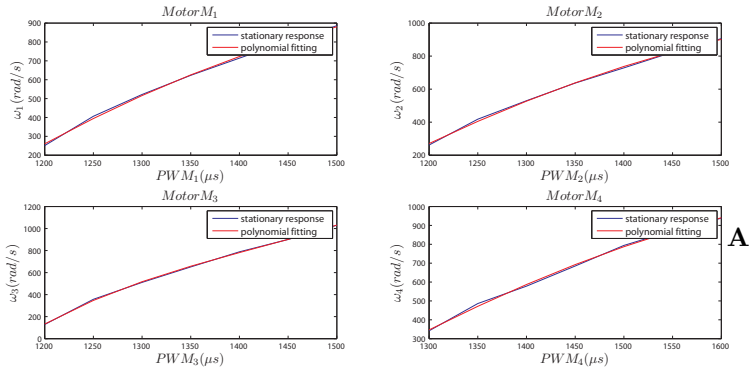

Fig. 5. Identification of the Actuators.

static gains of the motor models are then obtained linearizing the curves around the operating point. The linearization point and static gains are presented in Table II.

TABLE II
DEAD ZONE OF THE MOTORS

Motor	Linearization Point $PWM_i^0(\mu s)$	Static Gain $k_i((rad/s)/\mu s)$
M_1	1254.2	2.53
M_2	1250.0	2.56
M_3	1265.9	3.47
M_4	1322.9	2.53

All motors are considered to have the same time constant. To determine it, the tachometer is used to record the response of the motor to a PWM step. It is concluded that the $\tau = 0.162s$

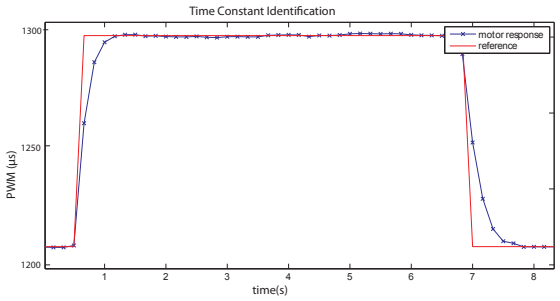

Fig. 6. Determination of the Time Constant of the Motor Set.

E. Linear State Space Model

After linearizing analytically and computationally the kinematics and dynamics model of the prototype, the model of the sensors and the model of the actuators, the linear state space model is obtained with the input vector $\mathbf{U} = \mathbf{PWM} = [PWM_1, PWM_2, PWM_3, PWM_4]^T$, the state vector is $\mathbf{X} = [\mathbf{V}, \mathbf{\Omega}, \mathbf{P}, \mathbf{\Psi}]^T$ and the output vector reduced to $\mathbf{Y} = [\overline{a}_x, \overline{a}_y, \overline{g}_x, \overline{g}_y, \overline{g}_z, \overline{N}_y]$ after noticing that $\overline{a}_z, \overline{N}_x$ and $\overline{N}_z$ had no effect on the system:

$$\mathbf{A} = \begin{bmatrix} 0 & 0 & 0 & 0 & 0 & 0 & 0 & 0 & 0 & 0 & -g_0 & 0 \\ 0 & 0 & 0 & 0 & 0 & 0 & 0 & 0 & 0 & g0 & 0 & 0 \\ 0 & 0 & 0 & 0 & 0 & 0 & 0 & 0 & 0 & 0 & 0 & 0 \\ 0 & 0 & 0 & 0 & 0 & 0 & 0 & 0 & 0 & 0 & 0 & 0 \\ 0 & 0 & 0 & 0 & 0 & 0 & 0 & 0 & 0 & 0 & 0 & 0 \\ 0 & 0 & 0 & 0 & 0 & 0 & 0 & 0 & 0 & 0 & 0 & 0 \\ 1 & 0 & 0 & 0 & 0 & 0 & 0 & 0 & 0 & 0 & 0 & 0 \\ 0 & 1 & 0 & 0 & 0 & 0 & 0 & 0 & 0 & 0 & 0 & 0 \\ 0 & 0 & 1 & 0 & 0 & 0 & 0 & 0 & 0 & 0 & 0 & 0 \\ 0 & 0 & 0 & 1 & 0 & 0 & 0 & 0 & 0 & 0 & 0 & 0 \\ 0 & 0 & 0 & 0 & 1 & 0 & 0 & 0 & 0 & 0 & 0 & 0 \\ 0 & 0 & 0 & 0 & 0 & 1 & 0 & 0 & 0 & 0 & 0 & 0 \end{bmatrix} \quad (13a)$$

$$\mathbf{B} = \begin{bmatrix} 0 & 0 & 0 & 0 \\ 0 & 0 & 0 & 0 \\ -0.0307 & -0.0310 & -0.0421 & -0.0307 \\ 0 & 1.0851 & 0 & -1.0743 \\ 1.0742 & 0 & -1.4713 & 0 \\ 0.0483 & -0.0488 & 0.0661 & -0.0483 \\ 0 & 0 & 0 & 0 \\ 0 & 0 & 0 & 0 \\ 0 & 0 & 0 & 0 \\ 0 & 0 & 0 & 0 \\ 0 & 0 & 0 & 0 \\ 0 & 0 & 0 & 0 \end{bmatrix} \quad (13b)$$

$$\mathbf{C} = \begin{bmatrix} 0 & 0 & 0 & 0 & 0 & 0 & 0 & 0 & 0 & 0 & -g_0 & 0 \\ 0 & 0 & 0 & 0 & 0 & 0 & 0 & 0 & 0 & g_0 & 0 & 0 \\ 0 & 0 & 0 & 1 & 0 & 0 & 0 & 0 & 0 & 0 & 0 & 0 \\ 0 & 0 & 0 & 0 & 1 & 0 & 0 & 0 & 0 & 0 & 0 & 0 \\ 0 & 0 & 0 & 0 & 0 & 1 & 0 & 0 & 0 & 0 & 0 & 0 \\ 0 & 0 & 0 & 0 & 0 & 0 & 0 & 0 & 0 & 0 & 0 & -1 \end{bmatrix} \quad (13c)$$

$$\mathbf{D} = \begin{bmatrix} -0.0559 & 0 & 0.0765 & 0 \\ 0 & 0.0564 & 0 & -0.0559 \\ 0 & 0 & 0 & 0 \\ 0 & 0 & 0 & 0 \\ 0 & 0 & 0 & 0 \\ 0 & 0 & 0 & 0 \end{bmatrix} \quad (13d)$$

Having all poles on the origin, the system is unstable. To validate that conclusion, the model is implemented in *Simulink*. The open loop response of the system confirms that the system is unstable.

III. ATTITUDE ESTIMATION

To compare the estimators, it is wished to have data concerning the angles. To obtain that, a 12 states LQR is used to close the loop and guarantee that the quadrotor follows a reference using ideal sensors as input data. The idea is to later use the data from that simulation to test the different estimators against the ideal data.

A. 12 states LQR Control

A 12 states controller is obtained with the weighting matrices of equation (14):

$$Q_{lqr} = diag([5, 5, 2, 100, 100, 50, 4, 4, 10, 150, 150, 60])$$
$$R_{lqr} = diag([0.01, 0.01, 0.01, 0.01]) \quad (14)$$

The states references are designed to excite all the states and dynamics of the system, it comprises X, Y, Z translations but also ψ rotations; some translations are performed while the quadrotor is rotated. Figure 7 presents the response of the system and the states references.

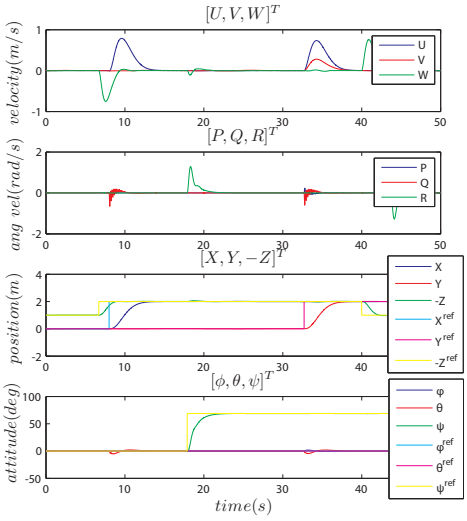

Fig. 7. Full-state Control Response.

An analysis of the closed loop system revealed that the controller stabilizes the system as suggested by having all the poles of the system in the left complex plan.

The data concerning the attitude of the quadrotor is used to evaluate two different complementary filters and then different Kalman filters.

B. Complementary Filters

The accelerometers are corrupted by high frequency noise. On the other side gyroscopes are affected by low frequency bias. The idea behind the complementary filter is to use this complementary behavior of the sensors. A low-pass filter applied to the accelerometers and a high-pass filter applied to the gyroscopes would retrieve the information concerning the attitude over the whole spectrum. As explained in [6], the complementary filter allows the fusion of low bandwidth position measurements with high bandwidth rate measurements. Equation (15) presents the general idea behind the complementary filter:

$$\begin{aligned}\widehat{\mathbf{X}} &= \frac{C(s)}{s+C(s)}\widehat{X}_{acc}(s) + \frac{s}{s+C(s)}\frac{\widehat{X}_{gyro}}{s} \\ &= T(s)\widehat{X}_{acc}(s) + S(s)\frac{\widehat{X}_{gyro}}{s}\end{aligned} \tag{15}$$

where: $\widehat{\mathbf{X}}$ is the estimated state vector; $\widehat{X}_{acc}$ is the estimation based on accelerometers; $\widehat{X}_{gyro}/s$ is the integration of the estimation based gyroscopes; $T(s)$ is a low pass filter; $S(s)$ is a high pass filter; and with the condition $T(s) + S(s) = 1$

1) First Complementary Filter: The filter designed at [7] uses explicit high and low pass filters to compute the sensor fusion and an algorithm to condition the sensor measurements. The first column of the direct cosine matrix, $\mathbf{S}$, corresponds to the projection of the North vector onto the body fixed frame; it is approximated to the compass measurement vector. The third column of the rotation matrix corresponds to the projection of the gravity vector thus to the accelerometers measurement vector, in a hover flight. Using the orthogonality property, the second column is obtained as the cross product of the two previous vectors. A renormalization procedure is applied to correct numerical errors. Finally using equation (16), the Euler angles are estimated.

$$\begin{aligned}\widehat{\phi} &= atan(\mathbf{S}(2,3), \mathbf{S}(3,3)) \\ \widehat{\theta} &= -asin(\mathbf{S}(1,3)) \\ \widehat{\psi} &= atan(\mathbf{S}(1,2), \mathbf{S}(1,1))\end{aligned} \tag{16}$$

The gyroscopes are numerically integrated to obtain the attitude estimation. First the Skew Symmetric Matrix is computed as equation (17) and then the rotation matrix is integrated as in equation (18) where a time update of the matrix is computed between in an interval T; I_3 is the identity matrix [3,3].

$$\Omega_\times = \begin{bmatrix} 0 & -\overline{g}_z & \overline{g}_y \\ \overline{g}_z & 0 & -\overline{g}_x \\ -\overline{g}_y & \overline{g}_x & 0 \end{bmatrix} \tag{17}$$

$$\mathbf{S_t} = (I_3 + T\Omega_\times)\mathbf{S_{t-T}} \tag{18}$$

The computed attitude from both sets of sensors are added after passing by the high pass filter and the low pass filter.

2) Passive Complementary Filter: The passive complementary filter presented in [2], [6] and [4] is based on the same logic as the previously described filter, but the formulation is slightly different. Let $\mathbf{R_s} = \mathbf{S}^T$ denote the transpose of the rotation matrix. The complementary filter can be written as:

$$\begin{aligned}\dot{\widehat{\mathbf{R}_\mathbf{s}}} &= \widehat{\mathbf{R}_\mathbf{s}}(\overline{\mathbf{\Omega}}^B + \omega_{corr})_\times - \omega_{bias})_\times \\ \omega_{corr} &= \lambda_1(\overline{\mathbf{N}}^B \times \widehat{\mathbf{R}_\mathbf{s}}^T \mathbf{N}^I) + \lambda_2(\overline{\mathbf{a}}^B \times \widehat{\mathbf{R}_\mathbf{s}}^T \mathbf{g}^I/g_0) \\ \dot{\omega}_{bias} &= -\lambda_i \omega_{corr}\end{aligned} \tag{19}$$

where: $()_\times$ defines the skew matrix operator as in equation (17). ω_{corr} is a correction term based on accelerometer and compass measurements. ω_{bias} is a bias correction term to eliminate the bias. Equation (16) is then also used to extract the attitude from the rotation matrix.

3) Discussion of the Complementary Filters: The estimations are compared to the real states generated by the control via 12 states LQR. The filters are implemented in a discrete mode. In Figure 8, the behavior of the two estimators without bias compensation term are shown.In Figure 9 the passive complementary filter is implemented with the bias compensation term.

The first complementary filter has only one variable to tune which weights the estimation bandwidth from the gyroscopes or both the accelerometer and the compass. The cut-off frequency is set to $1/T = 1/0.8$rad/s. The passive complementary filter has two parameters to independently control the importance given to the accelerometer and the compass: $\lambda_1 = 0.5$, $\lambda_2 = 0.6$ and $\lambda_i = 5$.

The passive complementary filter appears to be a finer method than the first filter; it allows a discriminate weighting of the individual sensors and is computationally more efficient to implement due to its lack of renormalization. On the other hand it is less intuitive.

Both filters depend on inverse trigonometric functions. As seen from the first complementary filter,the bias results in the

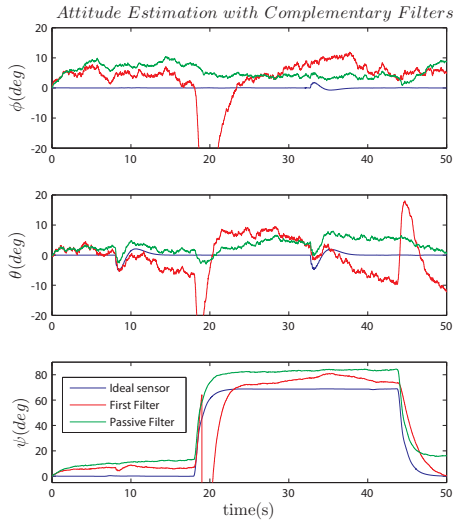

Fig. 8. Attitude Estimation with Complementary Filters.

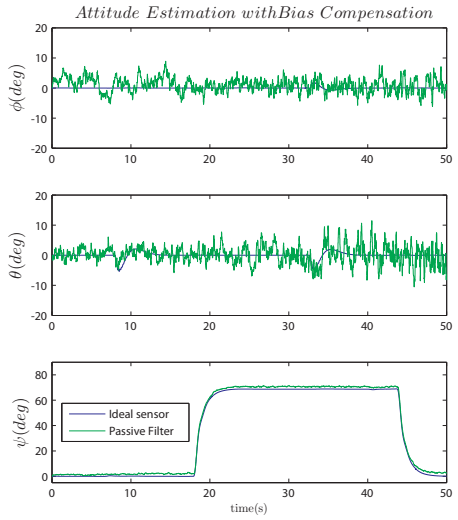

Fig. 9. Passive Filter with Bias Compensation.

estimation based on the gyroscopes to pass the non continuity of the $atan()$ function used to calculate the angle ψ.

Because of that non-continuity, the first complementary filter presents a worse estimation than the passive filter for the three angles. As a consequence only the passive filter was further investigated and implemented with bias compensation.

As seen from Figure 9, the bias compensation term appears to reduce greatly the error caused by the bias. However, the noise affecting ϕ and θ increases when compared to the situation without bias compensation. As a conclusion, it appears that the passive complementary filter is better than the first complementary filter (with the chosen set of parameters) but is still too dependent on trigonometric functions and struggles with the noise filtering.

C. Kalman Filters

An alternative to the complementary filters is to use the Kalman filter as done in [8], [9] and [10]. Consider the discrete linear system described by equation (20):

$$\begin{aligned} \mathbf{X_{k+1}} &= \mathbf{A}_d\mathbf{X_k} + \mathbf{B}_d\mathbf{U_k} + w_k \\ \mathbf{Y_k} &= \mathbf{C}_d\mathbf{X_k} + \mathbf{D}_d\mathbf{U_k} + v_k \end{aligned} \tag{20}$$

where: $\mathbf{A}_d, \mathbf{B}_d, \mathbf{C}_d, \mathbf{D}_d$ are the discrete state space matrices of the system. $\mathbf{X_k}$ is the state vector at time k. w_k and v_k are respectively the process and measurement noises.
Q_k and R_k denote the process and measurement noise covariances of the stochastic variables w_k and v_k.

The Kalman filter can be written as a set of mathematical equations (described by the diagram of Figure 10). First the filter acts as a predictor: it uses the model of the system, the current state and the input vector to predict the future state considering the covariance error; this is the time update phase. Then the measurement update phase will correct the predicted state and the estimated covariance error according to the measurements and its noise covariance. The Kalman gain K_k, weights the time prediction and the measurement correction.

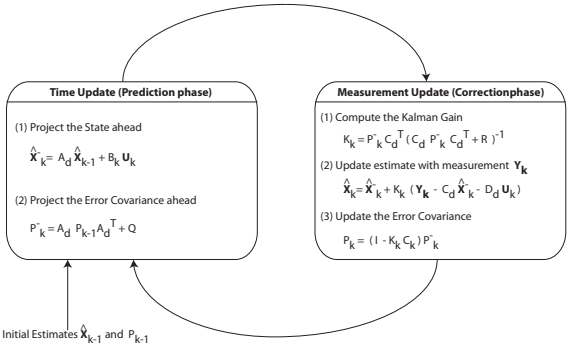

Fig. 10. Mathematical Formulation of the Kalman Filter[11].

1) Linear Kalman Filter: A first approach suggests using the full observable system with $\mathbf{Y} = [\overline{a}_x, \overline{a}_y, \overline{g}_x, \overline{g}_y, \overline{g}_z, \overline{N}_y]^T$, $\mathbf{X} = [P, Q, R, \phi, \theta, \psi]^T$ and the PWM signal as input variable.

The covariance matrices and initial covariance error matrix are taken using the noise characteristics of the sensors:

$$\begin{aligned} Q_k &= diag([.001, .001, 1, .001, .001, 10]) \\ R_k &= diag([0.09325, 0.08853, 0.245, 0.3012, 0.1961, 0.295]) \\ P_0 &= eye(6) \end{aligned} \tag{21}$$

This configuration of the Kalman filter is computationally heavy but provides the system with an estimation of the attitude and the angle rates.

2) Extended Kalman Filter: The EKF addresses the problem of estimating a state based on a non-linear model. The EKF linearizes the model about the current estimation; instead of using the matrices $\mathbf{A}_d, \mathbf{B}_d, \mathbf{C}_d, \mathbf{D}_d$, the nonlinear output and dynamic functions are used to linearize around the current state, resulting in the use of $\mathbf{A}_k$ and $\mathbf{C}_k$, obtained at each iteration. Figure 11 presents the algorithm.

According to [9] there is a possible improvement. Reminding the concept of the complementary filters, in which the gyroscope and the other sensors are treated separately, the idea of writing the model in a more compact form comes to mind. The complementary filters integrate the gyroscopes to "predict" the evolution of the the attitude and correct that prediction with the information from the accelerometer and the compass. Instead of using the PWM signal as the input vector, one can write the system so that the gyroscopes are taken as input vector as:

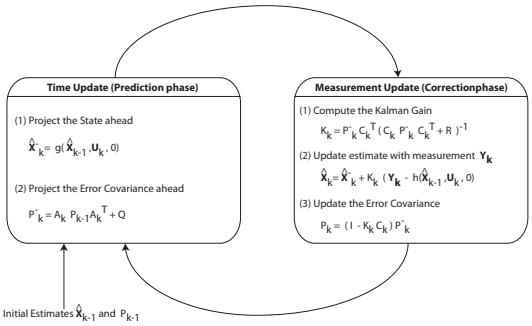

Fig. 11. Bloc Diagram of the EKF [11].

$$\dot{\mathbf{X}} = \begin{bmatrix} 0 & 0 & 0 \\ 0 & 0 & 0 \\ 0 & 0 & 0 \end{bmatrix} \mathbf{X} + \begin{bmatrix} 1 & 0 & 0 \\ 0 & 1 & 0 \\ 0 & 0 & 1 \end{bmatrix} \mathbf{U} \qquad (22)$$

where: $\mathbf{X} = [\phi, \theta, \psi]^T$. $\mathbf{U} = [P, Q, R]^T$.

However $\mathbf{C}_k$ will have to be defined at each step.

The algorithm is simple but requires the use of trigonometric functions for each iteration. The covariance matrices are presented by equation (23):

$$\begin{aligned} Q_k &= diag([.02, .02, 2]) \\ R_k &= diag(([0.09325, 0.08853, 0.245, 0.3012, 0.1961, 0.295])) \\ P_0 &= zeros(3) \end{aligned} \qquad (23)$$

3) Discussion of the Kalman Filters: The estimations obtained with the described methods are presented in Figure 12. The characteristics of the estimations are presented in Table III.

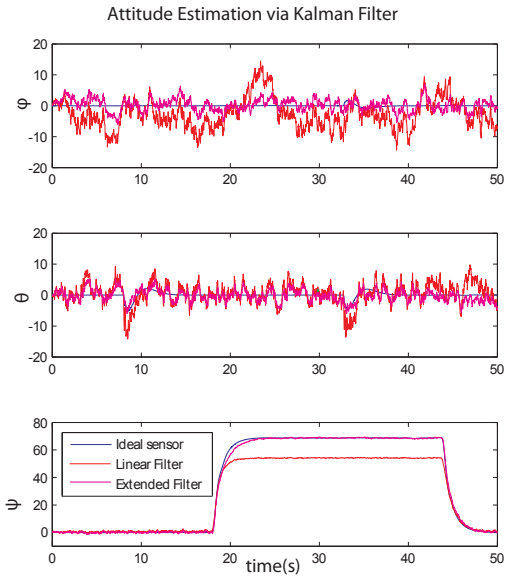

Fig. 12. Attitude Estimation with Kalman Filters.

The linear filter presents an impossibility of reaching an estimated angle over $57deg$. Indeed, the approximation $sin\psi = \psi$ is correct only for small angles around the linearization point. However since the trigonometric function is bounded, the approximation will also be bounded by $\psi < 1rad$, which explains the $57°$ bound.

The linear filter has the advantage of estimating all necessary states whereas the EKF has no processing on the angle rates. On the other side, the EKF is computationally more efficient and presents a better estimations; From Table III, the mean error is smaller using the EKF. Because it is a nonlinear method, the EKF is able to overcome the $\psi = 1rad$ limitation.

TABLE III
COMPARISON OF KALMAN FILTERS

Estimator	Estimated Angles					
	ϕ		θ		ψ	
	std (deg)	mean (deg)	std (deg)	mean (deg)	std (deg)	mean (deg)
Linear Filter	4.80	2.62	3.09	0.40	7.38	7.06
Extended Filter	2.02	0.33	1.78	0.12	1.02	0.13

From the different variations of the Kalman filter, one can conclude that the standard EKF is the best estimator. It is computationally more efficient than the EKF with bias estimation and it is able to overcome the linearization limits.

IV. ATTITUDE STABILIZATION

The Kalman filter has proven to be effective at attitude estimation in simulation. The behavior of the EKF is now tested on the prototype, to be fully validated, and in simulation with estimation feedback control.

A. Practical Implementation of the Estimator

To test the EKF on the prototype, two tests are undertaken: in the first, the prototype is held still, thus having $\phi = \theta = 0$ and $\psi(t) = 0$, with all motors on, and the behavior of the estimator is compared to the values presented in Table III. The estimated data is acquired and plotted in Figure 13. Table IV presents the mean estimated value for the attitude, $\widehat{\phi}$, and the standard deviation of the error. The objective is to test whether the implemented EKF is affected by any bias or not.

In a second test, the EKF is tested using different attitude references, to verify whether the implemented EKF is able to properly track the estimated attitude. The quadrotor is set horizontally, then it is moved to $\phi = 10°$ and $\theta = 0°$, and finally to $\theta = 10°$ and $\phi = 0°$. The results are presented in Table V, showing the standard deviation of the error and the mean measurement written $\widehat{\phi}$ for simplicity.

Finally, the yaw motion is tested separately: first the prototype is turned on and aligned with the magnetic North, then successively it is rotated to $\psi = 10°, 90°$ and $180°$. The results are presented in Table VI, showing the mean measurement and the standard deviation of the measurement.

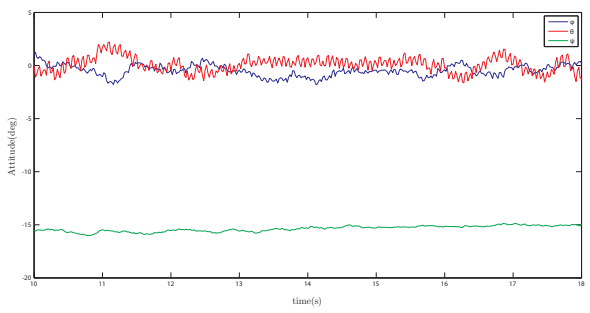

Fig. 13. Implementation of the Estimator.

TABLE IV
ATTITUDE ESTIMATION ERROR WITH NULL REFERENCE

ϕ			θ		
ϕ (deg)	$\widehat{\phi}$ (deg)	std (deg)	θ (deg)	$\widehat{\theta}$ (deg)	std (deg)
0	-0.452	0.547	0	0.099	0.715

Recalling from Table III the results obtained in simulation using the EKF, it is shown that the mean error of the estimation of ϕ, θ and ψ in simulation and in the implementation are similar: $0.30°$ for ϕ and $0.12°$ for θ in simulation, and $0.45°$ for ϕ and $0.1°$ for θ in the implementation. These mean values confirm that the initialization routine, which compensates for any constant bias, is efficient.

The standard deviation of the error are better in the implementation than in simulation. Indeed, for ϕ the simulation indicates a $2.02°$ standard deviation, which is greater than the $0.547°$ measured. The same result is seen regarding θ, where the simulation indicating $1.78°$ contrasts with the $0.715°$ measured The test shows that the EKF is not affected by any time varying bias; the EKF successfully filters out the noise affecting the sensors.

TABLE V
ATTITUDE ESTIMATION ERROR WITH DIFFERENT REFERENCES

ϕ			θ		
ϕ (deg)	$\widehat{\phi}$ (deg)	std (deg)	θ (deg)	$\widehat{\theta}$ (deg)	std (deg)
0	0.249	0.482	0	-0.103	0.649
10	10.32	0.514	0	-0.063	0.729
0	0.322	0.524	10	9.973	0.682

The values obtained in both tests are consistent. Indeed, the mean values and the standard deviation of the error concerning ϕ and θ are similar for the test where the prototype was kept horizontally, Table IV, and the test where the attitude is changed, Table IV. Therefore, the EKF proves to be efficient at updating the attitude during the motion of the prototype.

TABLE VI
HEADING ESTIMATION

ψ		
ψ (deg)	$\widehat{\psi}$ (deg)	std (deg)
0	1.629	0.297
10	10.550	0.278
90	92.572	0.287
180	186.302	0.331

Regarding the heading test: the mean values obtained in simulation are better than the mean values obtained with the implementation, which is justified by the difficulty in manually setting the heading. The values of the standard deviation of ψ are $1.02°$ in the simulation and $0.27°$ in the implementation. This test confirms the ability of the EKF to estimate the attitude, namely ψ.

These tests suggest that EKF is a suitable method for attitude estimation purposes. Moreover, because the EKF acts as predicted by the simulations, it suggests that the noise identification of the sensors models is correct.

B. 8 states LQR Control

The controller developed so far is based on the 12 states model and considers the ideal sensors; it was used to develop the estimation strategies and to tune the estimators. However, because the 12 states are not available since the model is not fully observable, a controller based on the 8 states model is designed to stabilize the quadrotor: to stabilize the quadrotor in a hovering flight 8 states are necessary: $\mathbf{X} = [W, P, Q, R, Z, \phi, \theta, \psi]^T$ and $\mathbf{U} = \mathbf{PWM}$. The stabilization problem corresponds to keeping the quadrotor hovering at a certain height. The model considered to obtain this controller is obtained from the initial 12 states model, eliminating the rows and columns corresponding to unnecessary states:

$$\dot{\mathbf{X}} = \begin{bmatrix} 0 & 0 & 0 & 0 & 0 & 0 & 0 & 0 \\ 0 & 0 & 0 & 0 & 0 & 0 & 0 & 0 \\ 0 & 0 & 0 & 0 & 0 & 0 & 0 & 0 \\ 0 & 0 & 0 & 0 & 0 & 0 & 0 & 0 \\ 1 & 0 & 0 & 0 & 0 & 0 & 0 & 0 \\ 0 & 1 & 0 & 0 & 0 & 0 & 0 & 0 \\ 0 & 0 & 1 & 0 & 0 & 0 & 0 & 0 \\ 0 & 0 & 0 & 1 & 0 & 0 & 0 & 0 \end{bmatrix} \mathbf{X} \tag{24a}$$

$$+ \begin{bmatrix} -0.0307 & -0.0310 & -0.0421 & -0.0307 \\ 0 & 1.0851 & 0 & -1.0743 \\ 1.0742 & 0 & -1.4713 & 0 \\ 0.0483 & -0.0488 & 0.0661 & -0.0483 \\ 0 & 0 & 0 & 0 \\ 0 & 0 & 0 & 0 \\ 0 & 0 & 0 & 0 \\ 0 & 0 & 0 & 0 \end{bmatrix} \mathbf{U} \tag{24b}$$

The 8 states LQR is designed in the discrete mode using the matrices presented in equation (25), which are discretized computationally.

$$\begin{aligned} Q_{lqr} &= diag([60, 5, 5, 20, 100, 10, 10, 30]) \\ R_{lqr} &= diag([0.01, 0.01, 0.01, 0.01]) \end{aligned} \tag{25}$$

Since the aim is to test the stabilization, the controller can be tested with estimation feedback: for this simulation the matrices of the estimator are re-tuned according to equation (26):

$$\begin{aligned} Q_k &= diag([.05.05.1]) \\ R_k &= diag([.2.2.05.05.1.01]) \end{aligned} \tag{26}$$

The EKF has also proven to provide accurate estimations of the attitude. It is now of interest to analyze the combination of both. Figure 14 presents the simulation, using $\mathbf{X_{ref}} = [0, 0, 0, 0, 0, -1, 0, 0, 0]^T$ as a reference and initial condition.

Table VII presents some characteristics of the attitude error.

TABLE VII
ATTITUDE ERROR

ϕ		θ		ψ	
std (deg)	mean (deg)	std (deg)	mean (deg)	std (deg)	mean (deg)
2.26	0.25	1.75	0.10	0.70	0.11

The high pass filter used to obtain the vertical velocity uses a cut-off frequency $1/0.005$rad/s.

This simulation suggests that the quadrotor could be stabilized for a hover flight using the chosen sensors and the implemented control and estimation methods. To further analyze

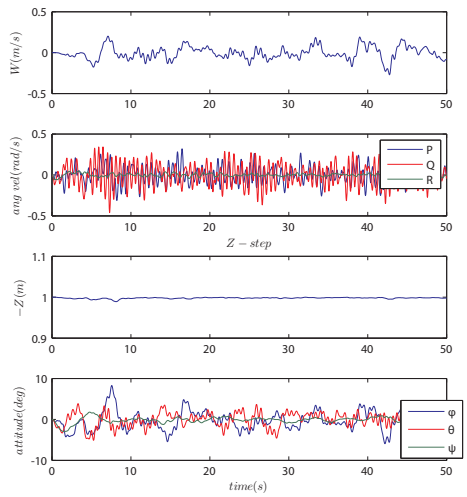

Fig. 14. Attitude Stabilization.

the stabilization of the attitude and altitude with estimation feedback, another test is proposed: setting the initial conditions to $0.2rad$ for the angles and $2m$ for the height keeping the same reference vector. The result is shown in Figure 15.

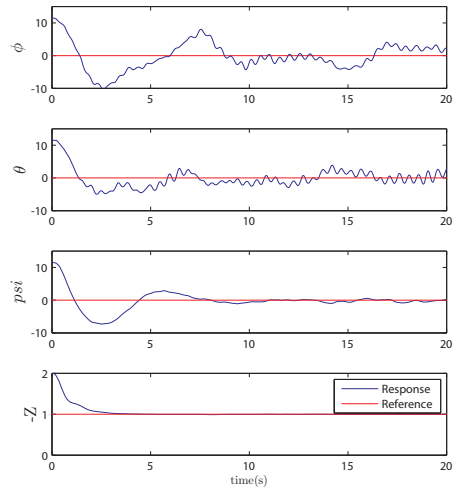

Fig. 15. Attitude Stabilization with different Initial Conditions.

The tests confirm that the LQR and EKF solution for attitude and height estimation are efficient methods.

V. Conclusions

With the aim of creating a functional platform, able to sustain an autonomous hovering flight with small drift in position and a stabilized flight when remotely controlled, different steps were reached:

- The model of prototype was obtained defining experimentally parameters.
- The sensors were modeled using real noise measurements corresponding to the flight conditions, therefore with all motors turned on.
- The model of the actuators was obtained considering the speed controllers, the propellers and the motors. The motors were approximated to a first order system; all motors were considered to have the same time constant which was obtained experimentally using a laser based tachometer to measure the angular speed of the propellers.
- Different estimation approaches were considered, namely complementary filters including the passive complementary filter and different Kalman filters as the linear and the extended Kalman filters. It was concluded that the EKF was the best estimator being insensitive to the bias of the gyroscopes contrarily to the other Kalman filters.
- An LQR controller based solely on the 8 observable states was then obtained and the EKF and the LQR were combined to stabilize the quadrotor. It was concluded that the estimation method and the control method were both efficient in simulation.
- Finally the EKF was implemented on the prototype. This validates the model of the sensors with the exception of the range finder which proved to be noisy.

Some improvements are left as further work:

- The speed controllers should be identical. This would greatly improve the performance of the controller.
- Different control techniques such as robust control and nonlinear control should be considered for future works.
- The estimation of the height should be done using a barometric sensor instead of an infra red sensor. The improvement would result in a better estimation of the height and a possible better estimation of the vertical velocity.
- It is left for future work the implementation of the controller and the actual flight. It is expected to be necessary some fine tuning of the controller to achieve a hover flight.
- Finally, the development of a position controller is left as future work.

References

[1] Samir Bouabdallah, Marcelo Becker, Vincent de Perrot, and Roland Siegwart. Towards obstacle avoidance on quadrotor. XII International Symposium on Dynamic Problems of Mechanics, 2007.

[2] Robert Mahony, Tarek Hamel, and Sung-Han Cha. A coupled estimation and control analysis for attitude stabilisation of mini aerial vehicles. Proceedings of the Australasian Conference on Robotics and Automation.

[3] Mark Euston, Paul Coote, Robert Mahony, Jonghyuk Kim, and Tarek Hamel. A complementary filter for attitude estimation of a fixed-wing uav. pages 340–345. International Conference on Intelligent Robots and Systems, 2008. IROS 2008. IEEE/RSJ, 2008.

[4] Robert Mahony, Tarek Hamel, and Jean-Michel Pflimlin. Nonlinear complementary filters on the special orthogonal group. volume 53 n-5, pages 1203–1218. IEEE Transactions on Automatic Control, 2008.

[5] C.Konvalin. *Compensating for Tilt, Hard Iron and Soft Iron Effect*, 2008.

[6] Robert Mahony, Tarek Hamel, and Jean Michel Pflimlin. Complementary filter design on the special orthogonal group so(3). pages 1477–1484. IEEE Conference on Decision and Control, 2005.

[7] William Premerlani and Paul Bizard. Direction cosine matrix imu: Theory. 2009.

[8] N.Shantha Kumar and T.Jann. Estimation of attitudes from a low-cost miniaturized inertial platform using kalman filter-based sensor fusion algorithm. 29:217235, 2004.

[9] R.Yadlin. Attitude determination and bias estimation using kalman filtering.

[10] David Haessig and Bernard Friedland. Separate-bias estimation with reduced-order kalman filters. volume 43, pages 983–987. IEEE Transactions on Automatic Control, 1998.

[11] Greg Welch and Gary Bishop. An introduction to the kalman filter. 2001.